1 **Supporting information for:**

2 **"A multi-instrumental approach for calibrating two real-time**

3 **mass spectrometers using high performance liquid**

4 **chromatography and positive matrix factorization"**

5 Melinda K. Schueneman[1], Douglas A. Day[1], Dongwook Kim[1], Pedro Campuzano-Jost[1], Seonsik

6 Yun[1], Marla P. DeVault[1], Anna C. Ziola[1], Paul J. Ziemann[1], and Jose L. Jimenez[1]

7 [1]Department of Chemistry and Cooperative Institute for Research in Environmental Sciences, University of

8 Colorado, Boulder, CO 80309, USA

10   **S1 General system information for multi-instrumental calibration method**
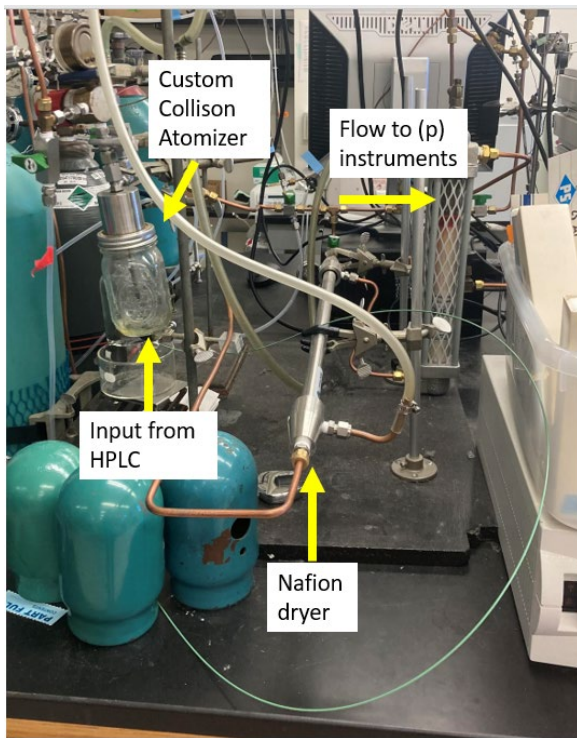
12   **Figure S1. HPLC tubing into custom atomizer**

14   **Table S1. Tube volumes, flows, and residence times from HPLC separation to particle instrument detection.**

Item	Total volume (mL)	Flow rate (flow through)	Residence time
Tubing transferring liquid from after HPLC column and UV-Vis detection to atomizer	0.67	1.0 mL min^{-1}	40 s
Atomizer	500	8-10 l min^{-1}	3-3.75 s
Nafion drier	7.0	~ 8 l min^{-1}	0.053 s
Tubing before manifold	118.3	7.2 l min^{-1}	1 s
Post manifold EESI	31.2	0.84 l min^{-1}	2.2 s
Post manifold AMS	14.1	1.5 l min^{-1}	0.6 s

Post manifold SMPS A	34.2	1.43 l min^{-1}	1.4 s
Post manifold SMPS B	28.5	1.49 l min^{-1}	1.2 s
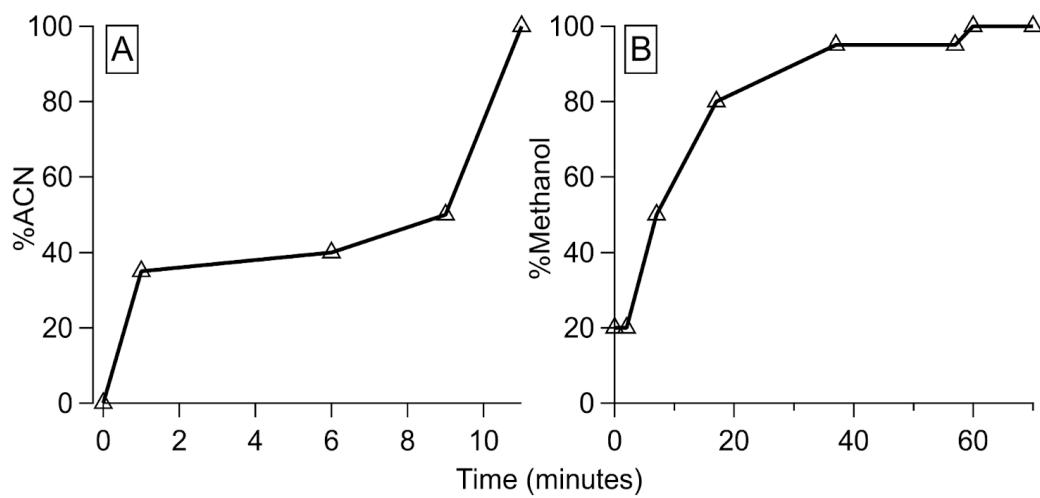
Figure S2. Solvent gradients for (A) standard HPLC runs and (B) β-pinene HPLC run. The other solvent was a mixture of 95% H$_2$O/5% ACN.

21 **Table S2. Standard compounds used for HPLC method demonstration, source and purity, volatility (calculated using**

22 **published vapor pressures), estimated percent evaporated during transmission (from atomizer output to detection,**

23 **calculated with C* and measured OA concentration at detection), and density (using the ratio of d_{va}/d_m)**

Species	Source + purity	Saturation Mass Concentration (μg m^{-3}) (T=298 K)	Estimated Percent Evaporated	Density
3-methyl-4-nitrophenol	Aldrich, 98%	5,210	92%	1.27**
Phthalic acid	Beantown Chemical, ACS grade, 99.5%	5.72	0%	1.05
4-nitrophenol	Aldrich, 99%	10,600	94%	1.48**
Succinic acid	Aldrich, 99%	1.21	0%	1.18
4-nitrocatechol	Alfa Aesar, 98%	64	63%	1.26
L-malic acid	Aldrich, 97%	0.24	-	1.28
Citric acid	Fisher Scientific	0.18	-	-
Levoglucosan	Chem-Impex Int'l, ≥99.0%	13*	-	1.30
Acetonitrile	Fisher Chemical, >99.95%	-	-	-
Methanol	Fisher Chemical, >99.9%	-	-	-
Water	VWR Chemicals, HPLC grade	-	-	-
Ethyl Acetate	Fisher Chemical, 99.5%	-	-	-

24 ***Reported in (Pagonis et al., 2021)**

25 ****Density of bulk solution from literature**

26 The densities measured using the d_{va}/d_m ratio do not match the literature values for bulk density well. This is

27 potentially due to different phases from that of the bulk material, and/or non-spherical particle shape (Jayne et al.,

28 2000; Huffman et al., 2005). Regardless, the d_{va}/d_m density was used as the best estimate here.

29
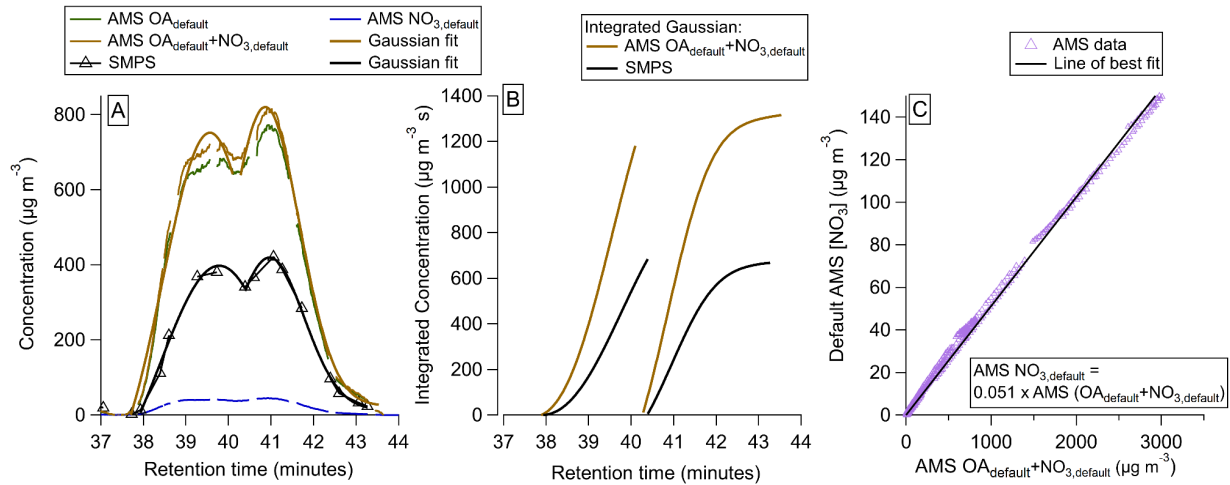
30

31 **Figure S3. (A) AMS default mass concentrations for [OA], [NO$_3$], and [OA+NO$_3$]; SMPS mass concentrations, corrected**

32 **for the average density. (B) Integrated Gaussian curves for each peak. (C) Default AMS [NO$_3$] vs total default AMS signal**

33 **[OA+NO$_3$], fit with a line. The slope (ratio of [NO$_3$]/[OA+NO$_3$])=0.051.**

34

35 The nitrate contribution to the total mass for this peak was ~5.1%. Fitting the bulk peaks (which are composed of

36 multiple eluents) may result in some error in the nitrate contribution approximation.

S2 SMPS testing and validation

S2.1 Fast scanning operation and validation

The fast scanning operation of the SMPSs was essential here. A "fast scan" here means 30 seconds for voltage scanning, with 10 seconds retrace time (when the voltage is returned back to 0). This allows for an SMPS data point to be obtained every 40 seconds, and when two SMPSs are used with interleaved timing, every ~20 seconds. This faster scanning is not without precedent; one paper published in 1990 first denoted the term "scanning electrical mobility spectrometer" or SEMS (Wang and Flagan, 1990). In that paper, researchers demonstrated that aerosol distributions for atmospherically relevant samples could be measured in a 30-second scan time, with a 30-second retrace time. This research led to the creation of new SMPSs that, like the SEMS, scanned continuously, and thus would be capable of 30s scanning times. A study a few years later put this to the test, and looked at the impact of changing SMPS scan times, and found that shorter scan times led to more smearing (less-resolved size distributions) and lower peak maximas (Russell et al., 1995). They suggest that this is driven by the residence time of the particles from the output of the DMA to the optical detection by the CPC (t_d). In addition, a paper in 2002 elaborated on the conclusions from Russell et. al. (1995), and found that when scanning with a flow rate of 0.3 l min^{-1}, combined with a 30 seconds scan time, the size distribution was significantly broadened (Collins et al., 2002). The maximum concentration was decreased by over 50% when compared to a longer scan time (300s), but the integrated concentration did not seem as affected, due to broadening in the faster scan.

Typically, SMPSs are run at longer scan times of two minutes or more (Sioutas, 1999; McMurry, 2000; Jeong and Evans, 2009). One study modified an SMPS by adding an aerosol particle mass analyzer (APM). With the modified system, data points were recorded every 60 seconds (Malloy et al., 2009). Another study, which took place on an aircraft and measured the air over Mexico City, ran their SMPS with a scan time of 1.5 minutes (DeCarlo et al., 2008). Despite the conclusions of Wang and Flagan (1990), many in the community run their SMPSs as "slow" (e.g. scan times of two or more minutes) instruments. Henceforth, "slow" will refer to the 2 minute scans, and "fast" will refer to the 30 second scans.

Here, we test each SMPS with a combination of "long" scans (2-minute scans, 15 s retrace, 3 l min^{-1} sheath flow) and "fast" scans (30 s scans, 10 s retrace, 6 l min^{-1} sheath flow). In order to assess the usability and accuracy of the fast scan method, tests were carried out (Fig. S4) to compare the total integrated volume concentration, number size distributions, and volume size distributions for two-minute scans at both a sample flow of 0.3 l min^{-1} and 1.5 l min^{-1}, and 30 second scans done with the same flow rates.

67
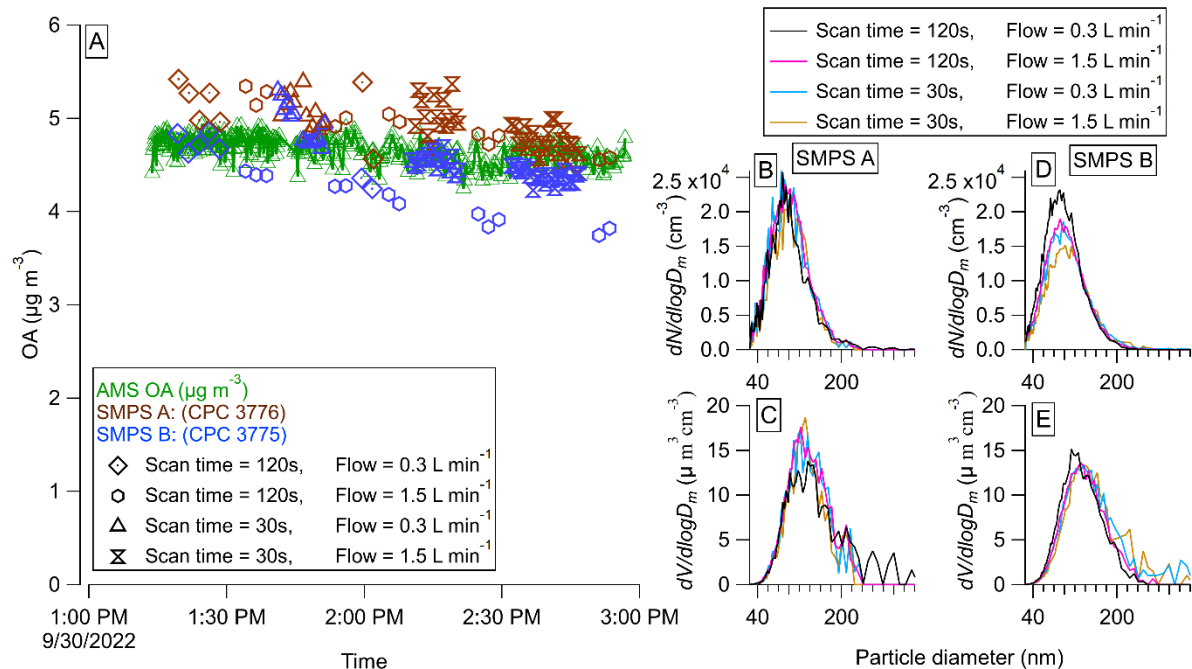
Figure S4. (A) Estimated particle mass concentration from SMPS A and B compared to the total OA measured by the AMS, for different combinations of scanning times and sample flow rates when sampling constant DOS concentrations from a large chamber. (B) Number distribution comparisons for different combinations of scanning times and flow rates for SMPS A, (C) Volume distribution comparisons, (D) number distribution comparisons for SMPS B, and (E) volume distribution comparisons for SMPS B.

73

In Fig. S4a, the total concentration of dioctyl sebacate (DOS) was measured by an AMS (green) and time averaged to 10 seconds. The AMS-measured DOS (after AMS calibration for that species) was used as the reference concentration. DOS was generated using a custom evaporation-condensation apparatus (Sinclair and La Mer, 1949; Krechmer et al., 2017)(Sinclair and La Mer, 1949), and flowed into a 20 m^3 Teflon chamber. To start, we scanned with both SMPSs set to a 2 minute scan time with a 15 second retrace time, and a flow rate of 0.3 l min^{-1}. This is typically how we run our SMPSs for laboratory studies and we have compared with even longer scans (up to 300 s, same flow settings) showing good agreement (Liu et al., 2019) and has shown good quantitative agreement for intercomparisons during chamber and field campaigns. Those "long scans" serve as a reference. Both SMPSs were run concurrently.

Some researchers show peak smearing when using faster scan times (although, those studies seem to use a sample flow rate=0.3 l min^{-1}) (Russell et al., 1995). These studies posit that the smearing is mainly due to instrument specific/plumbing delay times from the output of the DMA to the optical detection by the CPC (Russell et al., 1995). In Fig. S4b, the number distribution is shown for the different flow/scan time configurations for the SMPS A. The black distribution for all scans is the reference (120 scan, 0.3 l min^{-1}, resolution=10). For the number distribution,

88   the peak width for the reference is more narrow than for all other configurations. The difference is minor, however,

89   and not as large as in other reports.

90   In Fig. S4c, the volume distributions are compared. The reference scan has a lower maximum concentration

91   than the other configurations, which seems to go against previously published results. Over time, [DOS] measured

92   by the AMS decreases, due to chamber wall loss effects. To counter this, reference scans (120 scans, 0.3 l min^{-1}

93   flows) are carried out throughout the experiment. For reference, the SMPSs were run with 30s scans and 1.5 l min^{-1}

94   sample flows for the HPLC method proposed in the main text.

95   The distributions for SMPS B are more affected by the different configurations. This is unsurprising, as it

96   has a longer t_d than SMPS A (table S3), and likely is more representative of the systems studied in the research cited

97   above. In Fig. S4d, the number distribution for the reference scan has a higher maxima than the other scans. The

98   faster, high flow scan is the most different from the reference, and has both a lower maxima and a wider peak width

99   (resolution = 4). This matches previous findings (Collins et al., 2002), but this study shows a far less dramatic peak

100   shape difference than that shown therein. This finding could introduce some quantification error. In Fig. S4, the

101   volume distributions match fairly well for all configurations. A faster instrument (such as an optical particle counter)

102   would be ideal to obtain faster measurements, but the small diameter particles produced by the Collison atomizer

103   makes running those instruments impractical and prone to error (due to low detection efficiency at smaller size

104   particles).

105   For the multi-instrumental calibration experiments, SMPS A and SMPS B were offset by twenty seconds.

106   That allowed us to obtain a volume concentration every approx. 20 seconds. For comparing the response between

107   the two SMPSs, an experiment was done where SMPS A and SMPS B were run concurrently (Fig. S5). SMPS A

108   and SMPS B are shown to match within ~0%-10% (at the maxima). The consistency observed in Fig. S5 between

109   SMPS A and SMPS B provides increased confidence in the use of each instrument in "fast" mode.

110
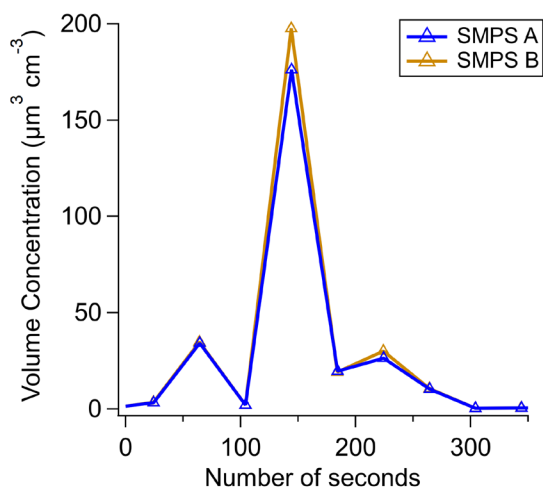
111

112   **Figure S5. Concurrent SMPS scans for an HPLC run**

 S2.2 SMPS delay time calculations

114 Delay times from the aerosol sampling manifold to the DMAs were calculated by running each DMA to size select
115 particles with a mobility diameter of 115 nm. Following transmission, the time it takes for the CPC concentration to
116 reach half of its maximum concentration ($t_{1/2}$) was calculated (table S3). Here, delay times were short, due to the
117 high sample flow. This does not eliminate the importance of having accurate delay times. Fast scans are often prone
118 to more error than their slow counterparts.

119 To calculate t_d (table S3), polystyrene latex spheres (PSLs) of a known diameter were atomized and
120 measured by the SMPSs. Calculating delay times ($t_{1/2}$ and t_d [delay time from exit of the DMA to the CPC]) allowed
121 us to properly align the slower SMPS measurements with the fast mass spectrometer measurements during the
122 relatively short chromatographically-separated compound peaks. Each eluting HPLC peak is only approx. 1.5
123 minutes long, and the instruments are run at different time resolutions. Each SMPS collects one data point every 40
124 seconds. For each data point, the SMPS software provided an uncorrected scanning start time. During the 40-second
125 scan, concentrations can change significantly. If the SMPS scan starts 15 seconds before the maxima is reached,
126 then the scan is recording concentrations at particle diameters both before, during, and after the peak maxima. If the
127 SMPSs were not corrected for their delay times, then the SMPS data point would show an erroneously low/high
128 concentration, and lead to errors when comparing to the other instruments.

129 **Table S3. Delay times for each SMPS. t$_{1/2}$ is the time it takes for the CPC concentration to reach half of its maximum**
130 **concentration**

SMPS name	CPC type	Delay time ($t_{1/2}$) (s)	DMA -> CPC delay time (t_d) (s)
SMPS A	3776	10.5	0.43
SMPS B	3775	8	1.55

131

132 **S3 Standard mixture mass spectra comparison for direct and multi-instrumental calibrations factors**

133 Mass spectra were obtained from PMF for many of the standards used in Sect. 3.2 and compared against the average

134 mass spectra from direct calibrations (Fig. S6).

135
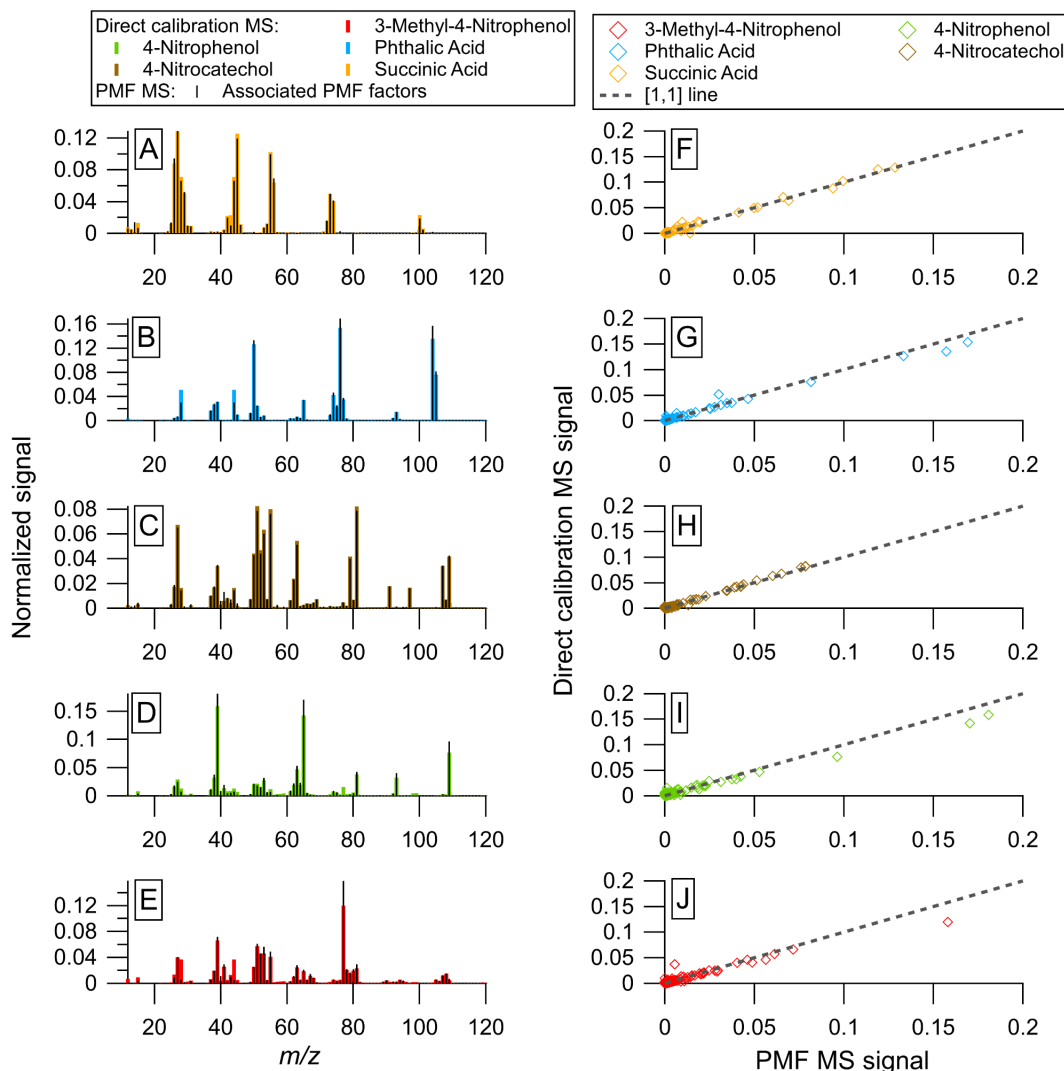
136

137 **Figure S6. (A)-(E) Mass spectra for monodisperse calibrations and associated PMF factors for species directly calibrated.**

138 **(F)-(J) scatter plot of MS signal at each measured *m/z* for the direct calibrations vs the PMF mass spectra.**

139

140 The uncentered correlation coefficients (table S4) match well between the assigned PMF factor mass spectra and the

141 corresponding direct calibration mass spectra.

142

143 **Table S4. Uncentered correlation coefficient (UC) between AMS direct calibration and PMF factor mass spectra (Ulbrich**
144 **et al., 2009)**

	Direct calibration MS				
PMF factor MS	Succinic Acid	Nitrocatechol	Phthalic Acid	Nitrophenol	3-methyl-4-nitrophenol
Succinic Acid	**0.99**	0.38	0.14	0.15	0.30
Nitrocatechol	0.38	**1.0**	0.23	0.49	0.62
Phthalic Acid	0.094	0.20	**0.99**	0.24	0.31
Nitrophenol	0.10	0.43	0.24	**0.99**	0.45
3-methyl-4-nitrophenol	0.21	0.58	0.27	0.49	**0.96**

145

146 The UC provides the same information as the dot product, without the need to normalize the mass spectra. For all
147 species, the UC>0.95. For nitrocatechol, the UC rounded up to 1.0 (near perfect agreement).

148   Similarly to the process carried out above, the mass spectra from the PMF solution for the data shown in
149 Fig. 6 was compared to direct calibrations (Fig. S7).

150

151
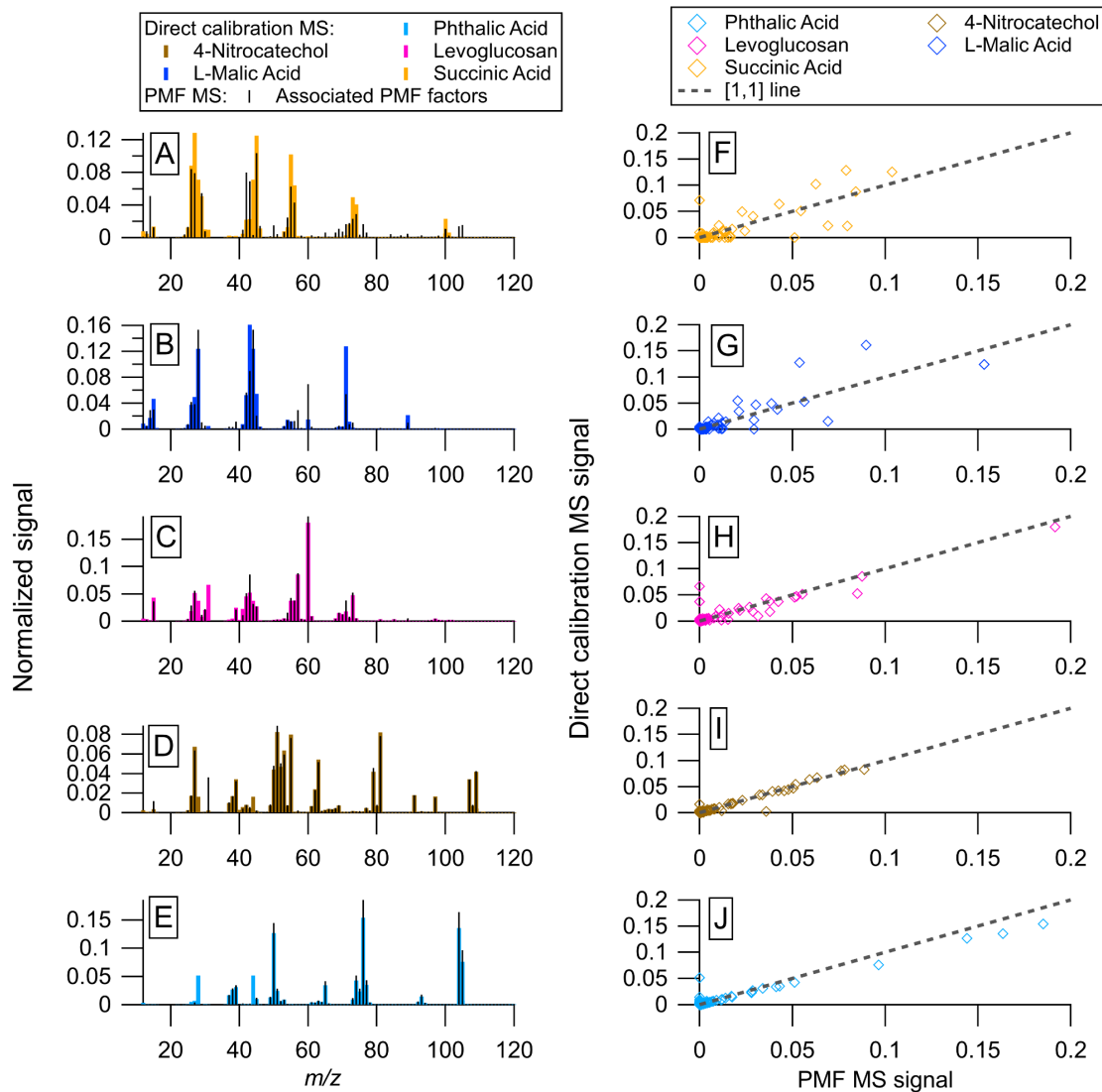
Figure S7. (A)-(E) Mass spectra for monodisperse calibrations and associated PMF factors for species directly calibrated

for the second standard solution (Fig. 6). (F)-(J) scatter plot of MS signal at each measured *m/z* for the direct calibrations

vs the PMF mass spectra.

155

Uncentered correlation coefficients were also calculated (table S5) and generally showed less agreement than those

shown in table S4.

158 **Table S5. Uncentered correlation coefficient (UC) between AMS direct calibration and PMF factor mass spectra (Ulbrich**
159 **et al., 2009) for standard solution 2 (Fig. 6, Fig. S7)**

	Direct calibration MS				
PMF factor MS	Succinic Acid	Malic Acid	Levoglucosan	Nitrocatechol	Phthalic Acid
Succinic Acid PMF	**0.81**	0.50	0.35	0.31	0.17
Malic Acid PMF	0.55	**0.89**	0.60	0.20	0.23
Levoglucosan PMF	0.36	0.41	**0.93**	0.19	0.029
Nitrocatechol PMF	0.33	0.12	0.23	**0.98**	0.20
Phthalic Acid PMF	0.030	0.014	0.025	0.19	**0.96**

160

161 Levoglucosan, nitrocatechol, and phthalic acid match well (UC>0.9). Succinic acid and malic acid match less well,
162 but still have a UC>0.8. As expected, the UC's for the second standard solution are less good than those for the first
163 standard solution (which was almost entirely resolved even without PMF).

164   **S4 β-pinene detailed information: density, molecular identification, PMF solution, and peak fitting**

165   For the SOA samples, the effective density was calculated as described in Sect. 2.5.2, shown in Fig. S8.

166
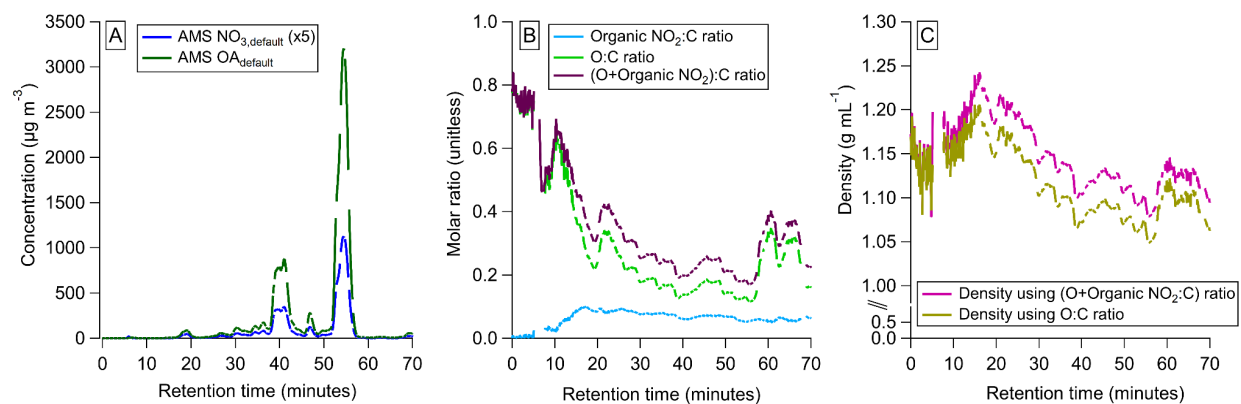
167

168   **Figure S8. (A) Measured NO₃ and OA from the AMS when sampling β-pinene+NO₃ SOA. (B) Atomic ratios for organic**
169   **nitrate:carbon, oxygen to carbon, and oxygen+organonitrates to carbon. (C) Estimated density from two approaches.**

170

171   The chromatogram from Claflin and Ziemann (2018) was compared to that measured here (Fig. 7), shown below in
172   Fig. S9.

173
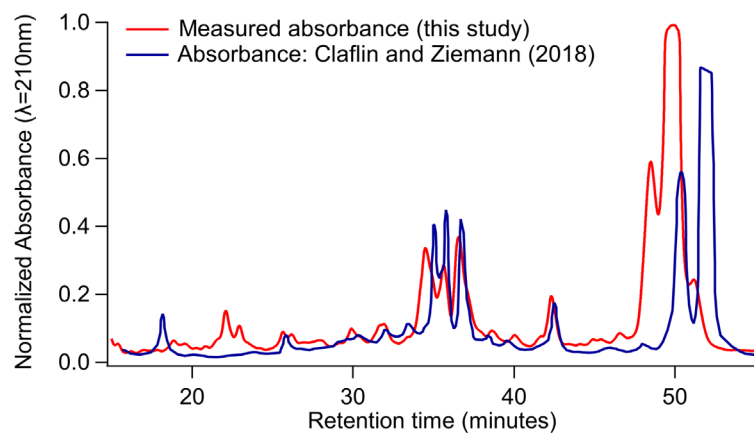
174

175   **Figure S9. Comparison to β-pinene chromatogram measured in Claflin and Ziemann (2018).**
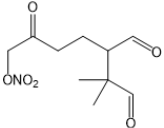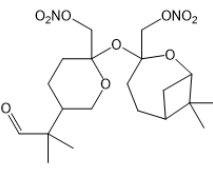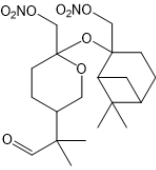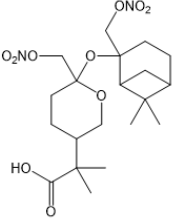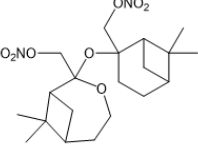
176

177   The chromatograms show the same general shape, although with slightly faster elution for this work. There are some
178   notable differences in the results between 20-30 minutes and 45-55 minutes. The final peak in the chromatogram

179 from Claflin and Ziemann is the same peak as the largest one measured here (retention time ~50 minutes). This
180 suggests that there could be some difference in the HPLC gradient method, or a potential contamination in one of
181 the HPLC solvents. Despite that, the overall signals are consistent, and some of the identified species are shown in
182 table S6.

183

184 **Table S6. Structure of known species (from Claflin and Ziemann (2018)), exact (theoretical) mass, observed mass**
185 **(measured with EESI+), and mass accuracy (based on EESI instrument multi-ion *m/z* calibration fit).**

Structure					
MW	245.23	460.48	444.48	460.48	428.48
Exact mass (+Na⁺) (Da)	268.0797	483.1955	467.2002	483.1955	451.2056
Detected mass (Da)	268.0879	483.1885	467.2032	483.1885	451.2120
Mass Accuracy (ppm)	30.6	-14.5	6.42	-14.5	14.2

186

187

188 PMF was run on the AMS data, shown below for the entire HPLC run (Fig. S10).

189

190
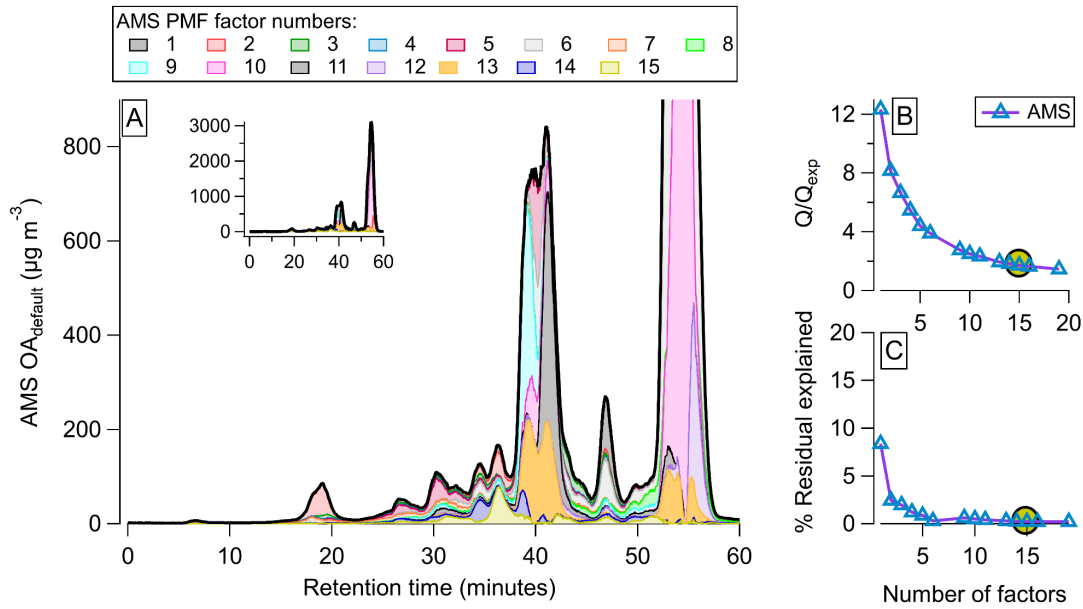
Figure S10. (A) stacked plot showing AMS PMF solution time series for the β-pinene/NO₃ SOA system, with inset showing

full scale. (B) Q/Q_expected, with the chosen solution (15 factors) circled. (C) Percent of the total sum of the residuals

explained, 15 factor solution circled.

A 15 factor solution was chosen. The time series and mass spectra for each factor are shown in Fig. S11.
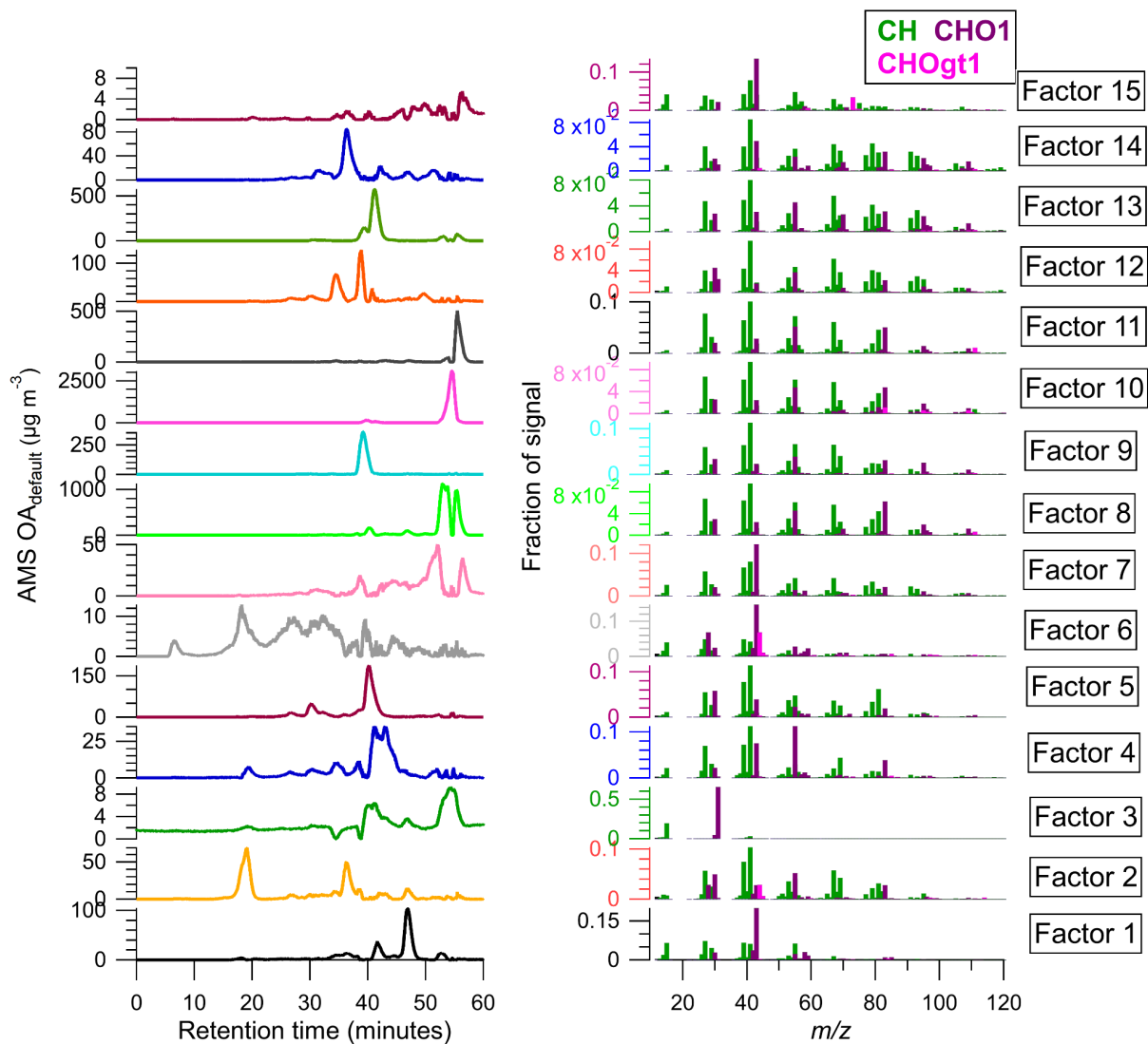
Figure S11. (Left) time series of individual PMF factors for the β-pinene + NO₃ SOA system and (right) HR mass spectra (colored by family) for each factor.

Many of the factors have different time series but very similar mass spectra. This suggests that the species fragment similarly in the AMS (and likely have similar phase states). The SOA products are mostly hydrocarbons with polar moieties (nitrate, carboxylic acids, ketones, and cyclic ethers). Many of the species retained the nonpolar moiety from injection to detection (as shown in the CH dominated mass spectra).

The peaks eluting from ~35 - ~43 minutes showed the strongest overlap (and also contained many of the known β-pinene/NO₃ SOA products). The time series for this portion of the HPLC run is shown in Fig. S12.
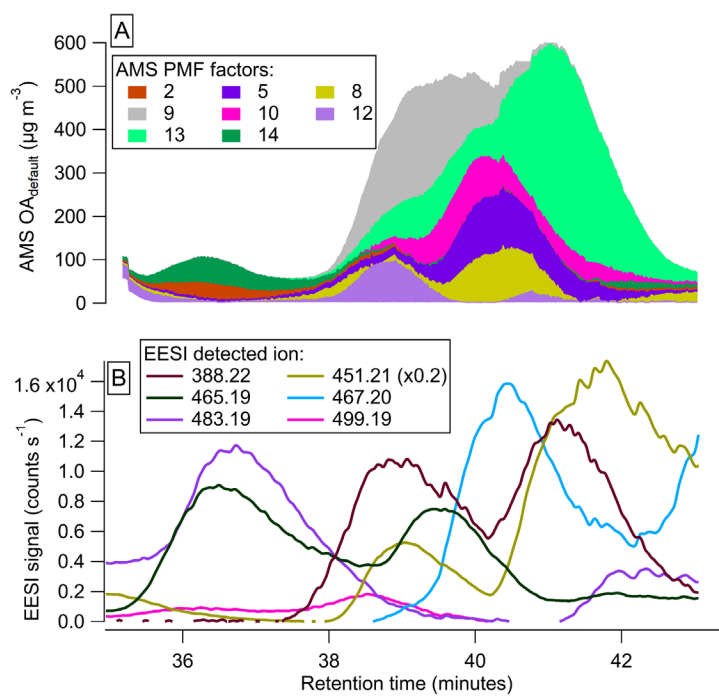
208

209 **Figure S12. (A) stacked plot of AMS PMF factors from 35-43 minutes and (B) EESI HR ions time series.**

210

211 As described in Sect. 3.3, EESI HR ions were matched to AMS PMF factors using the shape of the time series' as

212 well as the retention times. Individual peaks are shown in Fig. S13.

213

214

Figure S13. (a) *m/z*=268.1 **Gaussians, (b) integrals; (c)** *m/z*=388.2 **Gaussians, (d) integrals; (e) one peak for** *m/z*=451.2
Gaussians, (f) integrals; (g) one peak for *m/z*=451.2 **Gaussians, (h) integrals; (i)** *m/z*=465.2 **Gaussians, (j) integrals; (k)**
m/z=467.2 **Gaussians, (l) integrals; (m) one peak for** *m/z*=483.2 **Gaussians, (n) integrals; (o)** *m/z*=499.2 **Gaussians, (p)**
integrals. For the EESI HR ions, the total mass (Org+NO₃) was used in the denominator.

As described in Sect. 2.7, CF_x^E was determined either using the measured SMPS mass or the total AMS mass
(Org+NO₃). Fig. S13 shows the AMS OA mass, which was separated by PMF. As shown in Fig. S3, the NO₃
contribution to the total mass was ~5%. This contribution was added to the denominator to calculate CF_x^E which are
reported in table 2 in the main text.

224 **References**

225 Claflin, M. S. and Ziemann, P. J.: Identification and Quantitation of Aerosol Products of the Reaction of β-Pinene
226 with NO3 Radicals and Implications for Gas- and Particle-Phase Reaction Mechanisms, J. Phys. Chem. A, 122(14),
227 3640–3652, doi:10.1021/acs.jpca.8b00692, 2018.

228 Collins, D. R., Flagan, R. C. and Seinfeld, J. H.: Improved inversion of scanning DMA data, Aerosol Sci. Technol.,
229 36(1), 1–9, doi:10.1080/027868202753339032, 2002.

230 DeCarlo, P. F., Dunlea, E. J., Kimmel, J. R., Aiken, A. C., Sueper, D., Crounse, J., Wennberg, P. O., Emmons, L.,
231 Shinozuka, Y., Clarke, A. and Others: Fast airborne aerosol size and chemistry measurements above Mexico City
232 and Central Mexico during the MILAGRO campaign, 1foldr Import 2019-10-08 Batch 1 [online] Available from:
233 https://oaktrust.library.tamu.edu/bitstream/handle/1969.1/178622/document-2.pdf?sequence=2, 2008.

234 Huffman, J. A., Jayne, J. T., Drewnick, F., Aiken, A. C., Onasch, T., Worsnop, D. R. and Jimenez, J. L.: Design,
235 Modeling, Optimization, and Experimental Tests of a Particle Beam Width Probe for the Aerodyne Aerosol Mass
236 Spectrometer, Aerosol Sci. Technol., 39(12), 1143–1163, doi:10.1080/02786820500423782, 2005.

237 Jayne, J. T., Leard, D. C., Zhang, X., Davidovits, P., Smith, K. A., Kolb, C. E. and Worsnop, D. R.: Development of
238 an Aerosol Mass Spectrometer for Size and Composition Analysis of Submicron Particles, Aerosol Sci. Technol.,
239 33(1-2), 49–70, doi:10.1080/027868200410840, 2000.

240 Jeong, C.-H. and Evans, G. J.: Inter-Comparison of a Fast Mobility Particle Sizer and a Scanning Mobility Particle
241 Sizer Incorporating an Ultrafine Water-Based Condensation Particle Counter, Aerosol Sci. Technol., 43(4), 364–
242 373, doi:10.1080/02786820802662939, 2009.

243 Krechmer, J. E., Day, D. A., Ziemann, P. J. and Jimenez, J. L.: Direct Measurements of Gas/Particle Partitioning
244 and Mass Accommodation Coefficients in Environmental Chambers, Environ. Sci. Technol., 51(20), 11867–11875,
245 doi:10.1021/acs.est.7b02144, 2017.

246 Malloy, Q. G. J., Nakao, S., Qi, L., Austin, R., Stothers, C., Hagino, H. and Cocker, D. R.: Real-Time Aerosol
247 Density Determination Utilizing a Modified Scanning Mobility Particle Sizer—Aerosol Particle Mass Analyzer
248 System, Aerosol Sci. Technol., 43(7), 673–678, doi:10.1080/02786820902832960, 2009.

249 McMurry, P. H.: A review of atmospheric aerosol measurements, Atmos. Environ., 34(12), 1959–1999,
250 doi:10.1016/S1352-2310(99)00455-0, 2000.

251 Pagonis, D., Campuzano-Jost, P., Guo, H., Day, D. A., Schueneman, M. K., Brown, W. L., Nault, B. A., Stark, H.,
252 Siemens, K., Laskin, A., Piel, F., Tomsche, L., Wisthaler, A., Coggon, M. M., Gkatzelis, G. I., Halliday, H. S.,
253 Krechmer, J. E., Moore, R. H., Thomson, D. S., Warneke, C., Wiggins, E. B. and Jimenez, J. L.: Airborne extractive
254 electrospray mass spectrometry measurements of the chemical composition of organic aerosol, Atmospheric
255 Measurement Techniques, 14(2), 1545–1559, doi:10.5194/amt-14-1545-2021, 2021.

256 Russell, L. M., Flagan, R. C. and Seinfeld, J. H.: Asymmetric Instrument Response Resulting from Mixing Effects
257 in Accelerated DMA-CPC Measurements, Aerosol Sci. Technol., 23(4), 491–509,
258 doi:10.1080/02786829508965332, 1995.

259 Sinclair, D. and La Mer, V. K.: Light scattering as a measure of particle size in aerosols; the production of
260 monodisperse aerosols, Chem. Rev., 44(2), 245–267, doi:10.1021/cr60138a001, 1949.

261 Sioutas, C.: Evaluation of the Measurement Performance of the Scanning Mobility Particle Sizer and Aerodynamic
262 Particle Sizer, Aerosol Sci. Technol., 30(1), 84–92, doi:10.1080/027868299304903, 1999.

263   Ulbrich, I. M., Canagaratna, M. R., Zhang, Q., Worsnop, D. R. and Jimenez, J. L.: Interpretation of organic
264   components from positive matrix factorization of aerosol mass spectrometric data, Atmospheric Chemistry &
265   Physics, 9(9) [online] Available from: https://d-nb.info/114970523X/34, 2009.

266   Wang, S. C. and Flagan, R. C.: Scanning Electrical Mobility Spectrometer, Aerosol Sci. Technol., 13(2), 230–240,
267   doi:10.1080/02786829008959441, 1990.